JOURNAL OF MATERIALS SCIENCE 33 (1998) 1137–1143

Definition and measurement of the shear-lag parameter, β, as an index of the stress transfer efficiency in polymer composites

C. GALIOTIS, A. PAIPETIS
Materials Department, Queen Mary and Westfield College, University of London, Mile End Road, London E1 4NS, UK

The shear-lag parameter, β, employed in various problems of shear-lag analysis of composites is an unknown parameter which, in certain cases, is impossible to define. In this paper, a new methodology is proposed for the definition and subsequent experimental measurement of β for various single-fibre model composites. It is argued that, if β is defined as a fitting parameter for the solution of the shear-lag differential equation, then it can effectively serve as a stress-transfer efficiency index. The dependence of β upon the conditions prevailing at the fibre–matrix interface will be demonstrated by measuring β as a function of the fibre sizing in a carbon–epoxy composite system. © *1998 Chapman & Hall*

1. Introduction

It is well known that in fibre-reinforced composites the stress transfer process is activated at a discontinuity such as a fibre break or a fibre end. There have been a number of analytical models that attempted to derive analytical expressions for the fibre stress distribution over a given fibre length as a function of the applied stress, the fibre and matrix moduli and the type of geometry and/or testing configuration. The most commonly used method for the prediction of the stress transfer characteristics in composites is the so-called *shear-lag* method, which was proposed originally by Cox [1]. There are two sets of assumptions employed by Cox for the derivation of the axial stress in the fibre. The first set is concerned with the material parameters that are used for the formulation of the problem. These are as follows.

(i) The fibre and matrix behave as linear elastic solids.
(ii) The interface between the two components is perfect.
(iii) There is no load transfer through the fibre ends.

The second set of assumptions is concerned with the mathematical formulation of the problem. The most fundamental of those assumptions require that the radial displacement, u, with respect to x and the transverse normal stresses, $\sigma_{rr} + \sigma_{\theta\theta}$, are either zero or negligible [1–3]:

$$\frac{\partial u}{\partial x} \approx 0 \tag{1}$$

and

$$\sigma_{rr} + \sigma_{\theta\theta} \approx 0. \tag{2}$$

Cox [1] set out the whole problem by assuming that, if P is the load in the fibre at a fibre distance, x, then the rate of load transfer (or in other words the produced shear stress) at an applied far field strain, ε_m, is proportional to the difference between the axial displacement w, of the fibre, and the corresponding displacement, w_∞, that the matrix would undergo if the fibre were absent. The latter is in effect the axial displacement in the middle of a short fibre (for which its length is longer than the critical length) or the axial displacement of a continuous fibre. Hence

$$\frac{dP}{dx} = H(w - w_\infty) \tag{3}$$

where H is a proportionality constant which depends on geometrical and material parameters. In order to derive the constant, H, Cox [1] assumed that at a distance from the fibre axis equal to R_{Cox} the displacement of the matrix is, in fact, the unperturbed displacement w_∞. As stated by Nayfeh [2], Galiotis [4] and, more recently, Nairn [3], for single-fibre model composites, the parameter, R_{Cox}, can be defined as the radius of a matrix cylinder beyond which there is no influence of the fibre upon the deformation of the matrix.

The final one-dimensional equation derived by Cox [1] for the axial fibre stress, $\sigma_f(x)$, can be written as

$$\frac{\partial^2 \sigma_f(x)}{\partial x^2} - \beta^2 \sigma_f(x) = -\beta^2 \sigma_{f,\infty} \tag{4}$$

In fact, even more rigorous shear-lag analyses [2, 3] based on axisymmetric elasticity equations for two concentric cylinders (e.g., single-fibre model composites), rather than Equation 1, can also be shown [3] to lead to equation 4. However, the term β derived by Nayfeh [2] differs considerably from that derived by Cox [1]. Regardless of that for a cylindrical fibre of

length, l, radius, r, and modulus, E_f, Equation 4 can be easily solved to yield

$$\sigma_f(x) = E_f\varepsilon_\infty\left(1 - \frac{\cosh[\beta(l/2 - x)]}{\cosh(\beta l/2)}\right) \quad (5)$$

where ε_∞ is the far-field strain and β is the shear-lag parameter which has units of inverse length and depends on the material properties and the geometrical foundation of the problem.

Equation 3 can be simplified to

$$\sigma_f(x) = E_f\varepsilon_\infty[1 - \cosh(\beta x) + \tanh(1/2\beta l)\sinh(\beta x)] \quad (6)$$

The function $\tanh(1/2\beta l)$ takes the value of unity for any value of $\beta l \geqslant 10$. For all short-fibre composites for which $l \geqslant 2000\,\mu m$ and $\beta \geqslant 0.005$, then, from Equation 4,

$$\sigma_f(x) = \sigma_{f,\infty}[1 - \cosh(\beta x) + \sinh(\beta x)]$$

or

$$\sigma_f(x) = \sigma_{f,\infty}[1 - \exp(-\beta x)] \quad (7)$$

where $\sigma_{f,\infty}$ is the corresponding axial stress in the middle of the fibre.

In terms of strain values, Equation 7 can be written as

$$\varepsilon_f(x) = \varepsilon_\infty[1 - \exp(-\beta x)] \quad (8)$$

The significance of Equations 7 and 8 is that, for short fibres, the stress or strain distributions in the elastic region can be adequately predicted for a number of fibre–matrix combinations by just treating β as an *inverse length* fitting parameter rather than attempting to define it analytically. However, it is worth reiterating here that best results are obtained only if $\beta l \geqslant 10$.

As is now well known, experimental stress or strain profiles can be obtained on single-fibre, as well as multiple-fibre composites with the use of the technique of laser Raman spectroscopy. This technique is based on the stress sensitivity of the vibrational modes of almost all high-performance fibres, such as carbon or Aramid, and allows measurement of axial fibre stress with a resolution of the order of 1 μm [4–6]. From Equations 5 and 6, it is evident that, since laser Raman spectroscopy can provide $\sigma_f(x)$ and $\varepsilon_f(x)$ for any x (as well as $\sigma_{f,\infty}$ and ε_∞), the value of transfer length, l_0, for which $x = l_0 = 1/\beta$ can be found from the experimental axial stress or strain profiles at corresponding values of $0.63\,\sigma_{f,\infty}$ or $0.63\,\varepsilon_\infty$. Alternatively the shear-lag parameter, β, can be obtained by fitting an exponential curve of the form of Equation 7 or 8 to the experimental fibre stress or strain data, respectively.

In this paper, we have attempted the determination of β on short-fibre model composites made of sized and unsized carbon fibres and an epoxy resin. The short-fibre coupon geometry is ideal for these measurements because at low applied strains both fibre and matrix behave elastically and the interface is intact [7], hence, the first two shear-lag assumptions are satisfied. In addition, it has been found experimentally [8] that at least in the case of carbon fibre composites there is no measurable transmission of normal stresses through the ends of the fibre (assumption 3). However, it is worth mentioning here that in the case of Aramid–epoxy composites it is almost impossible to ascertain whether normal stresses are transmitted through the fibre ends owing to the damage caused by the cutting procedure [9, 10]. For all the fibre–matrix combinations examined here, the carbon fibre lengths were approximately 3 mm.

2. Experimental programme

2.1. Materials and specimen preparation

Two surface-treated high-modulus fibres produced by Soficar (France) were used in this study. One of the fibres, coded M40B-40B (MEBS), was supplied by the manufacturers with an epoxide sizing. The other fibre, M40B (MUS), was supplied unsized. Both fibres had an effective diameter of 6.6 μm (determined by density measurements) and a modulus of 390 GPa.

The epoxy resin used in this work was the two-part MY-750–HY-951 epoxy system provided by Ciba–Geigy. The resin (MY-750; unmodified liquid epoxy resin) and hardener (HY-951; triethylene tetramine) were mixed at 40 °C at a ratio of 4:1 and then degassed for 10 min under full vacuum. To produce short-fibre coupons [7], a thin layer of resin was first poured into the dogbone silicon rubber mould; then, the fibre was placed and aligned on top; finally, the rest of the mould was filled with resin. The preparation procedure is shown schematically in Fig. 1.

The composite coupons were cured for 2 h at 60 °C, removed from the moulds and subsequently post-cured at 120 °C. All dogbone specimens were ground until the embedded fibre was approximately 100 μm away from the surface and then polished. A strain gauge of gauge factor of 2.1 was attached to the resin surface and the applied strain was derived from the resistance measurements using a digital multimeter.

2.2. Specimen testing and Raman spectra acquisition

Raman spectra were taken with the remote Raman microprobe developed in house [11]. As shown in Fig. 2, the collected Raman light was guided through an optical fibre to a Spex 1000M single monochromator. The Raman signal was collected via a Wright Instrument charge-coupled device (CCD) and stored in a PC-compatible computer. By stressing single filaments in air, the stress sensitivity of the M40 fibres was found to be $-3.0\,cm^{-1}\,GPa^{-1}$ [12].

The short-fibre coupons were mounted on a Hounsfield universal testing machine and strained at distinct strain levels up to 0.6%. No fibre fractures were recorded. For all strain increments, Raman measurements were taken from both ends of the fibre and up to a distance of about 250 μm along the fibre and away from either end. Laser Raman sampling was carried out at steps of 2 μm at the vicinity of the fibre ends (from 0 to about 60 μm) and then at steps of 4 μm (from about 60 to 140 μm) and, finally, at steps of 10 μm (from 140 to 250 μm) 300 μm.

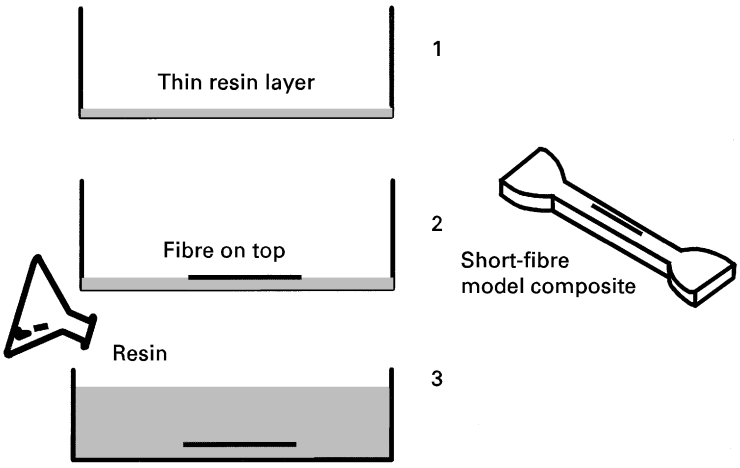

Figure 1 Specimen preparation procedure for short fibre model composites.

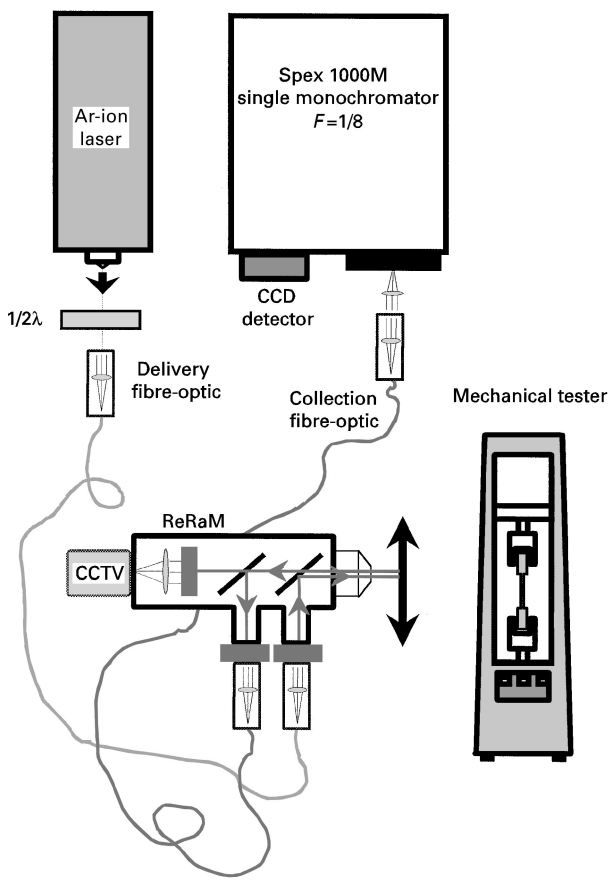

Figure 2 Remote Raman microprobe (ReRaM) (laser) set up employed for *in-situ* measurements of specimens deformed on the mechanical tester. CCTV; closed-circuit television.

3. Results and discussion

3.1. Measurement of the shear-lag parameter, β

In Figs 3 and 4, the axial fibre stress distribution is shown along the fibre for the sized and unsized systems, respectively. As can be seen, prior to the application of tensile stress, both MEBS and MUS fibres are subjected to axial compression owing to the thermal mismatch between the fibre and the matrix [13]. The magnitude of these stresses is a function of the temperature of mixing and gelation of the resin, as well as the curing and post-curing temperatures. For a single-fibre model composite, the overall axial compressive strain in the fibre reflects the amount of one-dimensional shrinkage in the resin. Since the matrix is isotropic, one can easily calculate the values of volumetric shrinkage, which are 0.5% and 0.7% for the sized (Fig. 3) and unsized (Fig. 4) systems, respectively [14]. The difference in the two values reflects, most probably, variations in the temperature of mixing and gelation, which is operator dependent. The most striking result, however, is that the stress built up in the short fibre is also shear dominated; the axial stress is zero at the end of the fibre and reaches its far-field value at some distance away from it.

Both systems are subjected to two increments of applied tensile strain of 0.3% and 0.6%. As can be seen in Figs 3 and 4, at 0.3% strain the compressive stresses have now been removed and the fibre stress distributions fluctuate around zero. At an applied strain of 0.6% the fibre stress distributions are now purely tensile and again the fibre stress is zero at the fibre end and reaches its maximum value at some distance away from it. It is worth adding here that the fibre stress distributions are not as smooth as in the case of the compressive stress built up (0% applied strain). Particularly in the case of the MEBS–MY-750 system, there is a gradual drop in the fibre stress values beyond a distance of 150–200 μm from the fibre ends. As explained in detail elsewhere [15], this is a result of the superposition of an axial tensile stress upon a fibre which is in a three-dimensional state of compressive stress (Fig. 5). In particular, the change in sign of interfacial shear that is required for the transition from axial compression to axial tension is gradual and, therefore, certain hysteresis can be observed near the middle of the fibre. This also explains why a tensile strain of 0.3% is required to annul compressive strains of -0.17% and -0.23% for the sized and unsized systems, respectively.

Regardless of the complexity of the stress transfer profiles, the methodology proposed in this paper for the determination of β is relatively simple. For any given fibre stress distribution within the elastic region, the value of β is derived by (a) measurement of $\sigma_{f,\infty}$ or ε_{∞} and (b) fitting an exponential curve of the form of Equation 7 or 8 to the raw data. The values $\sigma_{f,\infty}$ or

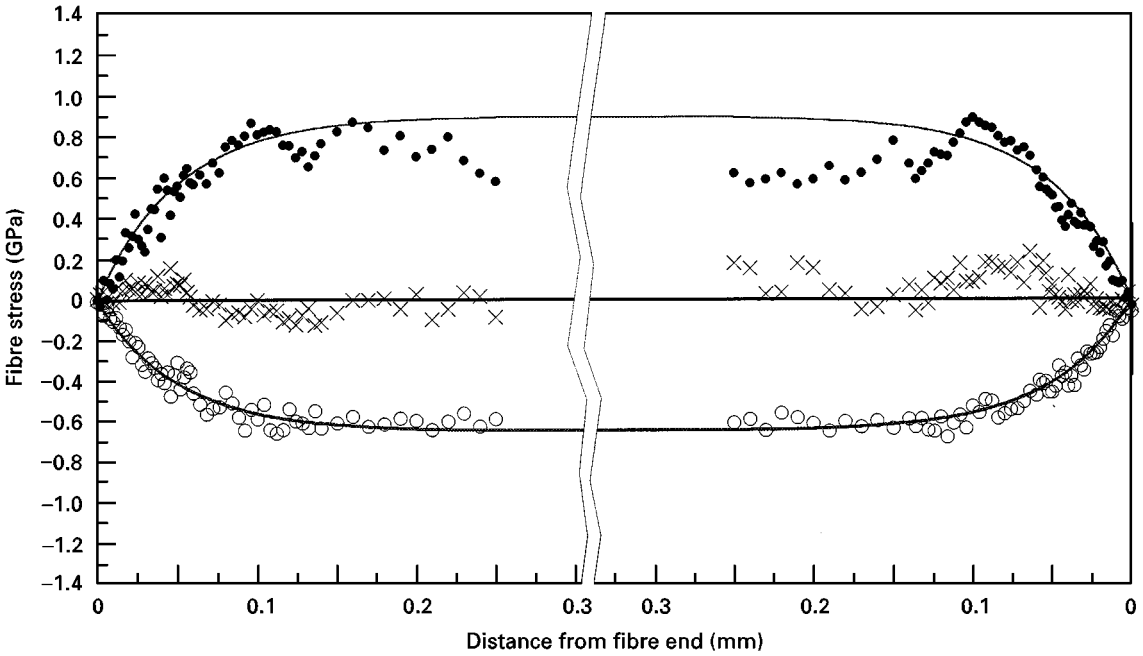

Figure 3 Axial fibre stress as a function of distance from fibre end for the MEBS (sized)–MY-750 system at 0.0% (○), 0.3% (×) and 0.6% (•) applied composite strains. The solid curves at 0.3% and 0.6% strain represent best fits of Equation 5 through which the values of the parameter, β, were derived.

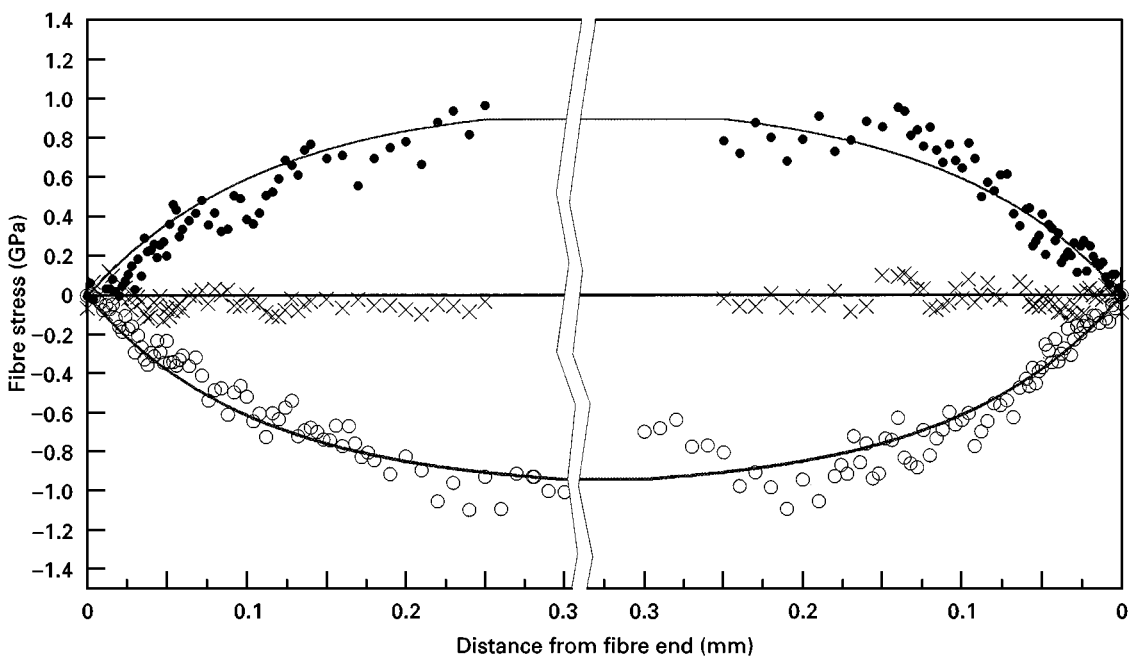

Figure 4 Axial fibre stress as a function of distance from fibre end for the MUS (unsized)–MY-750 system at 0.0% (○), 0.3% (×) and 0.6% (•) applied composite strains. The solid curves at 0.3% and 0.6% strain represent best fits of Equation 5 through which the values of the parameter, β, for the unsized system were derived.

ε_∞ have to be determined from the fibre stress or strain distributions by averaging the fibre stress or strain values at the middle of the fibre or at a distance well over the transfer length. This way any hysteresis between applied composite strain (measured by strain gauges) and actual fibre stress or strain in the fibre does not affect the value of β.

The solid curves in Figs 3 and 4 correspond to fits based on Equation 7. The values of β derived this way are given in Table I. Since for the MEBS–MY-750 and MUS–MY-750 systems the results obey the assumption $\beta l \geqslant 10$, then Equation 7 is valid. The average β values are of the order of 0.02 μm^{-1} and 0.009 μm^{-1} for the sized system and unsized systems, respectively. It is interesting to note that, within experimental error, the value of β does not change significantly with strain level (Table I) and is, therefore, considered to be a true reflection of the elastic response of each system. The fitted curves represent very well the data points at 0% applied strain (fibre in compression), whereas in the case of 0.6% strain the deviations are observed particularly at the middle of the MEBS fibre (Fig. 3). The

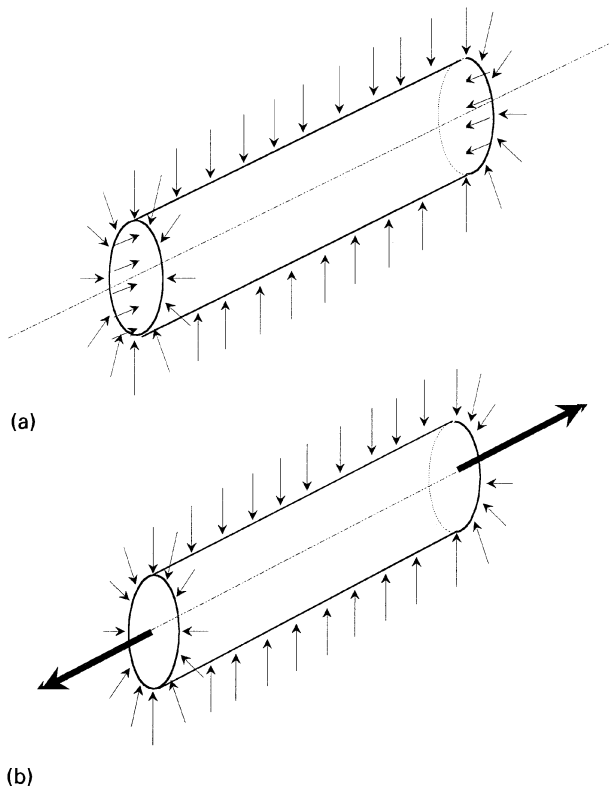

Figure 5 Schematic diagram of superposition of stress fields in the short fibre: (a) 0% applied strain, thermal stress field; (b) after the application of axial tensile stress.

reason for this discrepancy is the complexity of the stress field as the system is forced to undergo a shear generated compression-to-tension transition [15]. However, the overall picture is satisfactory and in systems where the residual fibre compression is minimal or non-existent (e.g., high volume fraction composites and cold-cured single-fibre composites), the proposed method should yield excellent fits. In conclusion, it has been demonstrated that the shear-lag parameter, β, can be used as an index of the stress transfer efficiency of the system as it is extremely sensitive to the conditions prevailing at the interface. In the case examined here, the addition of epoxide sizing to an identical MUS fibre has brought about an increase in β by a factor of 2.2.

3.2. Interfacial shear stress distributions

The exact equilibrium relationship between axial fibre stress, $\sigma_f(x)$, and interfacial shear stress (ISS), τ_{rx}, is given by

$$\tau_{rx} = -\frac{r}{2}\frac{\partial\sigma_f(x)}{\partial x} \tag{9}$$

An ISS distribution for the fitted axial stress profiles of Figs 3 and 4, can be obtained by combining Equations 7 and 9 provided that $\beta l \geqslant 10$

$$\tau_{rx} = -\frac{r\sigma_\infty\beta}{2}\exp(-\beta x) \tag{10}$$

The results for the two systems normalized by the far-field stress, σ_∞, are given in Fig. 6. As can be seen, the stress transfer responses of the two systems are considerably different: (a) the sized system indicates a considerably higher ISS value at the discontinuity ($x = 0$); (b) the decay of the ISS is more pronounced in the case of the sized system. Evidently, at the location of the fibre end ($x = 0$) the maximum ISS attained by the two systems will differ by a factor equal to β, which is 2.2 in the case examined here. Finally, it is worth mentioning that the predicted values of ISS for the maximum measured far-field stress are 29.8 MPa and 15.0 MPa for the sized and unsized systems at 0.9 GPa and 1.0 GPa far-field stress, respectively. These values are well below the interfacial shear strength of these systems which is measured by independent fragmentation experiments to be 41.9 ± 3.5 GPa and 36.8 ± 5.7 GPa for the sized and one unsized system respectively [6]. Hence, one can safely assume that the elastic limits have not been exceeded and that the interface is intact.

3.3. Matrix shear modulus, G_m^R, and effective volume fraction, R_{cox}/r

As mentioned earlier, the shear lag parameter, β, can be treated as an *inverse length* fitting parameter that satisfies the differential Equation 4. It is worth examining now why β is such a sensitive index of the stress transfer efficiency. The simplest expression for β has been derived by Cox based on the assumptions mentioned earlier and, in particular, Equation 3:

$$\beta = \left(\frac{2G_m^R}{r^2E_f\ln(R_{Cox}/r)}\right)^{1/2} \tag{11}$$

For single-fibre model composites the parameter, G_m^R, defines the shear modulus of the matrix cylinder of radius, R_{Cox}. The value of G_m^R is undoubtedly affected by the interphase chemistry (fibre surface treatment, fibre sizing, presence of matrix oligomers, etc.) which, in turn, will affect the value of β. Furthermore, the extent of the matrix cylinder of radius, R_{Cox}, beyond which the matrix flows as if the fibre were absent is also affected by the induced shear perturbation and thus cannot be considered as a constant. Therefore in Equation 11 we have two unknown parameters which affect the value of β.

TABLE I Values of β

System	Applied strain (%)	β (left) (μm^{-1})	β (right) (μm^{-1})	Far-field fibre stress (GPa)
MEBS–MY-750	0	0.0235	0.0192	− 0.65
	0.6	0.0213	0.0191	0.9
MUS–MY-750	0	0.0095	0.0094	− 1.0
	0.6	0.0082	0.0099	1.0

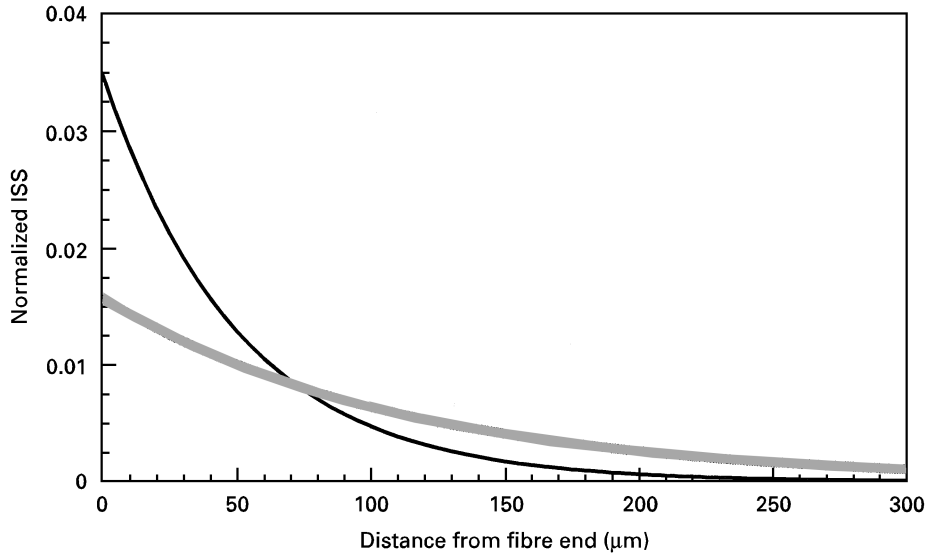

Figure 6 Predicted normalized interfacial shear as a function of distance from fibre end. The solid curves represent Equation 7 for values of β of 0.02 μm^{-1} and 0.009 μm^{-1} for the sized (■) and unsized (□) systems, respectively.

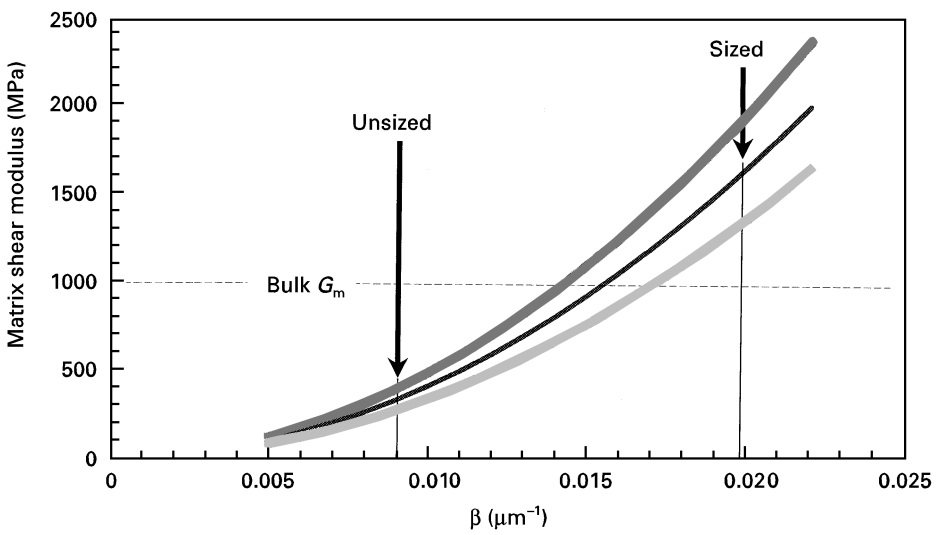

Figure 7 Prediction of average shear modulus of matrix cylinder of radius, R_{Cox}, as a function of β for three different R/r ratios of 5 (□), 7 (■) and (□) 10. The local shear moduli for the sized and unsized systems (values of β or 0.02 μm^{-1} and 0.009 μm^{-1}, respectively) are indicated.

An independent method to estimate the R_{Cox}/r ratio has appeared recently through the work on two-dimensional composites [17]. By placing the individual fibres far apart, a critical distance, R, has been defined over which there is no fibre–fibre interaction or, in other words, shear field perturbation. The value of R/r for a similar sized MUS fibre–epoxy system was found to be equal to about 9 [17]. Since R in that case corresponds to the centre-to-centre interfibre distance, then it follows that for the sized system that

$$\frac{R_{Cox}}{r} = \frac{1}{2}\frac{R}{r} = 4.5 \qquad (12)$$

In Fig. 7 the interfacial modulus G_m^R is plotted as a function of β for three different R_{Cox}/r values of 5, 7 and 10. As can be seen, the presence of sizing at the interface appears to increase somewhat the matrix shear modulus (of radius, R_{Cox}), yielding a more efficient system. For the unsized system and for all values of R_{Cox}/r, the matrix shear modulus appears considerably lower than its bulk value (Fig. 7). Lack of efficient cross-linking and/or precipitation of epoxide oligomers at the vicinity of the interface can account for the observed effect. The higher predicted shear modulus is indicative of the presence of a variation in local properties, which may result at an increase in the local matrix stiffness by 40% ($R_{Cox}/r = 5$). Assuming an equivalent increase in the local matrix shear strength, then one should expect a higher ISS for that system, which is in agreement with the relatively high ISS values predicted in the previous section.

4. Conclusions

The shear-lag parameter, β, has been defined for all shear-lag approaches. It has been demonstrated that the parameter, β, can be treated as an inverse length

fitting parameter for the solution of the main shear-lag differential equation. Thus, a simplified form of the normal fibre stress function has been derived for short fibres provided that $\beta l \geqslant 10$. Measurements of β were conducted on two identical fibre–matrix systems that incorporated sized and unsized fibres. The results demonstrated the suitability of β as an index of the efficiency of stress transfer in the two systems.

References

1. H. L. COX, *Brit. J. Appl. Phys.* **3** (1952) 72.
2. A. H. NAYFEH, *Fibre Sci. Technol.* **10** (1977) 195.
3. J. A. NAIRN, *Mech. Mater.* **26** (1997) 63.
4. C. GALIOTIS, *Compos. Sci. Technol.* **42** (1991) 125.
5. L. S. SCHADLER and C. GALIOTIS, *Int. Mater. Rev.* **40** (1995) 116.
6. A. PAIPETIS and C. GALIOTIS, *Composites A* **27** (1996) 755.
7. C. GALIOTIS, *Compost. Sci. Technol.* **48** (1993) 15.
8. N. MELANITIS, C. GALIOTIS, P. L. TETLOW and C. K. L. DAVIES, *J. Mater. Sci.* **28** (1993) 1648.
9. H. JAHANKHANI and C. GALIOTIS, *J. Compos. Mater.* **25** (1991) 609.
10. C. VLATTAS and C. GALIOTIS, in "Developments in the science and technology of composite materials", Proceedings of the Fifth European Conference on Composite Materials, Bordeaux, edited by A. R. Bunsell, J. F. Jamet and A. Massiah (European Association for Composite Materials, Bordeaux, 1992) pp. 415–420.
11. A. PAIPETIS, C. VLATTAS and C. GALIOTIS, *J. Raman Spectrosc.* **27** (1996) 519.
12. C. GALIOTIS, V. CHOHAN, A. PAIPETIS and C. VLATTAS, "Interfacial measurements in single and multi-fiber composites using the technique of laser Raman spectroscopy", ASTM Special Technical Publication 1290, edited by C. J. Spragg and L. T. Drzal (American Society for Testing and Materials, Philadelphia, PA, 1996) pp. 19–33.
13. C. C. CHAMIS, "Mechanics of load transfer at fibre–matrix interface", National Aeronautics and Space Administration Report TN D-5367 (1972).
14. I. M. ROBINSON, R. J. YOUNG, C. GALIOTIS and D. N. BATCHEDLER, *J. Mater. Sci.* **22** (1987) 3642.
15. L. S. SCHADLER, N. MELANITIS, C. GALIOTIS, J. C. FIGUEROA and C. LAIRD, *ibid.* **27** (1992) 1663.
16. V. CHOHAN and C. GALIOTIS, *Composites A* **27** (1996) 881.
17. *Idem.*, *Compos. Sci. Technol.* **57** (1997) 1089.

Received 15 August
and accepted 24 September 1997